# Electronic supplementary information

# Porous Cu nanosheets for efficient ammonia production via nitrate electroreduction

Eman-Shaiba Thani,[a] Yi-Ting Yang,[a] Qiu-Yu Du,[b] Rou Yuan,[a] Yong-Qi Zhang,[a] Yu-Tong Yan,[a] Xuan Ai,*[b] Yu Chen[b] and Shu-Ni Li*[a]

[a] Key Laboratory of Macromolecular Science of Shaanxi Province, School of Chemistry and Chemical Engineering, Shaanxi Normal University, Xi'an 710062, PR China.

[b] School of Materials Science and Engineering, Shaanxi Normal University, Xi'an 710062, PR China.

*Corresponding authors

E-mail: lishuni@snnu.edu.cn (S.-N. Li).

E-mail: aixuan@snnu.edu.cn (X. Ai).

## Experimental section

### Physical characterization

The chemical component, morphology, chemical state, crystallographic structure, surface area of electrocatalysts were characterized by scanning electron microscope (SEM, SU-8020), transmission electron microscopy (TEM, TECNAI G2 F20) with energy dispersive X-ray spectroscopy (EDX) accessory, X-ray diffraction (XRD, DX-2700), and X-ray photoelectron spectroscopy (XPS, Kratos Analytical Ltd.). The measurement of the concentration of $NH_3$ was completed using previous reported methods, which were performed on ultraviolet-visible spectrophotometer (UV-vis, UV-2600).

### Electrochemical measurements

All electrochemical tests were performed at the CHI 760E electrochemical workstation using a three-electrode or two-electrode system. In the three-electrode system, the working electrode is a glassy carbon electrode, the reference electrode is a saturated calomel electrode (SCE), and the auxiliary electrode is a carbon rod. All potentials were about the reversible hydrogen electrode (RHE), where $E_{RHE} = E_{SCE} + 0.242\ V + 0.0591\ pH$. The ink was prepared by adding 4 mg of catalyst to a mixture solution of 1.6 mL of water, 0.4 mL of isopropanol, and 10 μL of Nafion. 12 μL of catalyst was uniformly coated on the working electrode and dried at room temperature. The catalyst loading on the working electrode was about 0.3429 mg $cm^{-2}$.

**The Faradaic efficiency of $NO_3RR$ and $NH_3$ yield**

The chronoamperometry tests of $NO_3RR$ were performed under an H-type electrolytic cell, where the electrolyte was to be purged with Ar for 30 minutes prior to the test. The cathode and anode chambers were 40 mL of 0.5 M $Na_2SO_4$ + 0.05 M $NaNO_3$ solution and 0.5 M $Na_2SO_4$ solution, respectively.

The Faradaic efficiency for $NH_4^+$ production was defined as charge converted to $NH_4^+$ divided by the total charge passed through the electrodes during the electrolysis (Q), which was calculated according to the following formula:[1]

$$\text{Faradaic efficiency} = \frac{enF}{Q} \times 100\% \quad (1)$$

*e* was the number of electrons involved in the reaction; *n* was the quantity of the formed $NH_4^+$; *F* was the faraday constant (96,485 C $mol^{-1}$).

The $NH_4^+$ yield was calculated by following formula: [2]

$$\text{Yield rate} = \frac{n}{mt} \quad (2)$$

where *n* was the quantity of the formed $NH_4^+$ and *m* and *t* were the electrocatalyst mass and the reduction reaction time, respectively.

The Faraday efficiency of $NO_2^-$ to $NH_3$ can be calculated by the following formula:

$$FE_{NO_2^-} = (2 \times F \times c_{NO_2^-} \times V)/(46 \times Q) \quad (3)$$

The $NO_2^-$ yield can be calculated by the following formula:

$$\text{Yield}_{NO_2^-} = (c_{NO_2^-} \times V)/(m \times t) \quad (4)$$

$c_{NH_3}$ is the mass concentration of $NH_3$ (aq), V is the volume of electrolyte in the cathode compartment (20 mL), t is the electrolytic time (3 h), F is the Faradaic constant (96485

C $mol^{-1}$), Q is the total charge passing the electrode, m and t are the electrocatalyst mass and the reduction reaction time, respectively.

**Determination of $NH_4^+$-N**

Phenol hypochlorite method was used to detect the $NH_3$ concentration. [2] Firstly, the corresponding calibration curve was obtained by UV-vis curves for known concentration of $NH_4^+$ in 0.05 M $Na_2SO_4$. After running chronoamperometry test for 3 h, 500 μL were taken from the electrolyte and put it into the centrifuge tube and diluted to 5 mL with water. Then Stock reagents were added in solution and stand for 3 h. Finally, $NH_4^+$-N concentration was calculated according to the UV-vis curve and calibration curve.

**Determination of nitrite**

The concentration of $NO_2^-$ was detected by the N-(1-naphthyl) ethylenediamine spectrophotometry method. Take 1.0 mL electrolyte in a 50 mL volumetric bottle, dilute it with a little deionized water, then add 1.0 mL p-aminobenzene sulfonamide and mix well. After leaving for 2-8 min, add 1.0 mL N-(1-naphthyl) ethylenediamine dihydrochloride and mix well. Finally, after 10 min, the absorbance was measured by a UV-vis spectrophotometer at 540 nm wavelength. The concentration-absorbance curve was made using a series of standard sodium nitrite solutions.

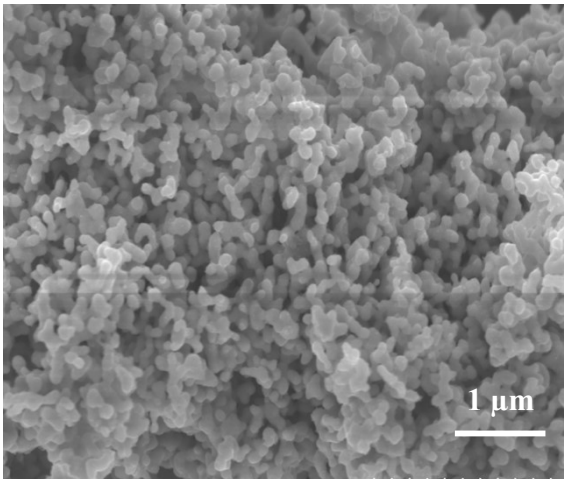


**Fig. S1.** SEM image of the Cu NPs.

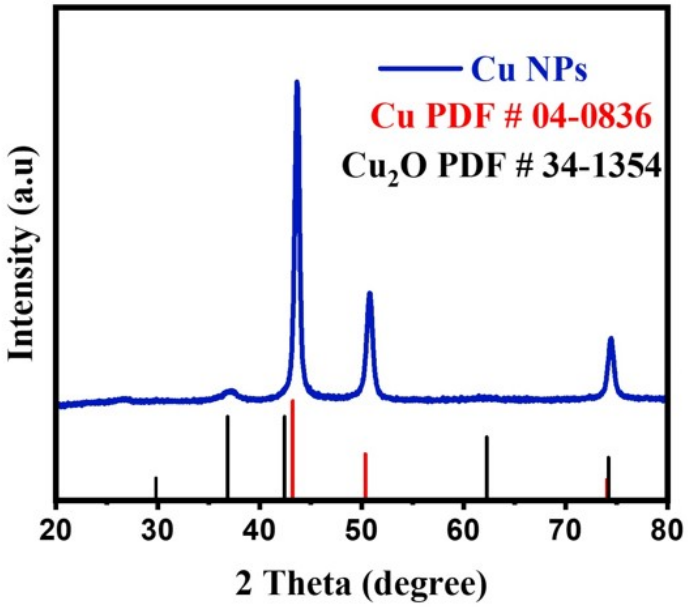


**Fig. S2.** XRD pattern of Cu NPs.

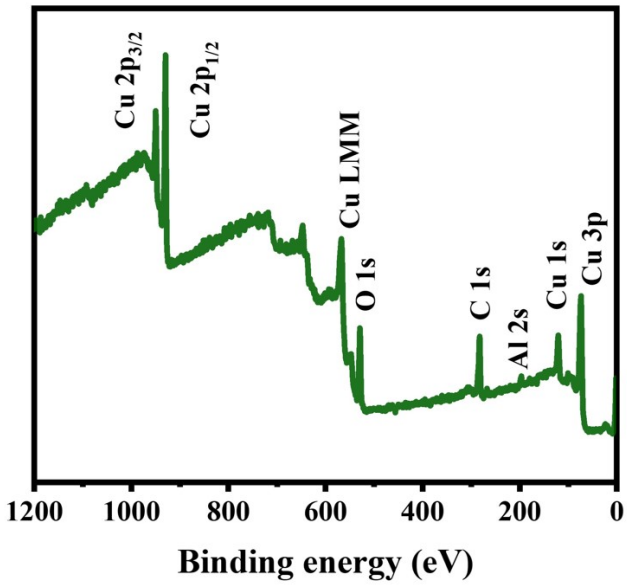


**Fig. S3.** XPS survey spectrum of Cu NPs.

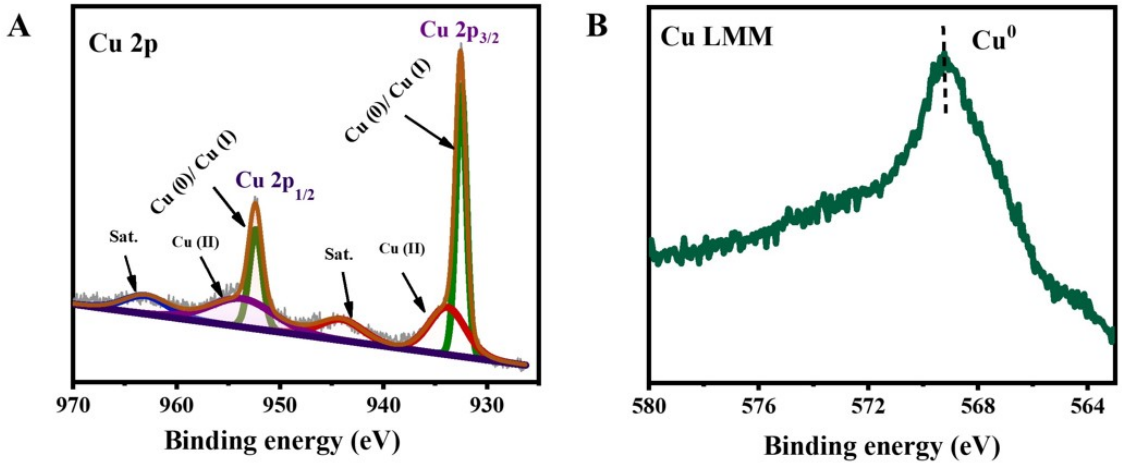


**Fig. S4.** (A) Cu 2p XPS spectra, (B) Cu LMM auger spectra of Cu NPs.

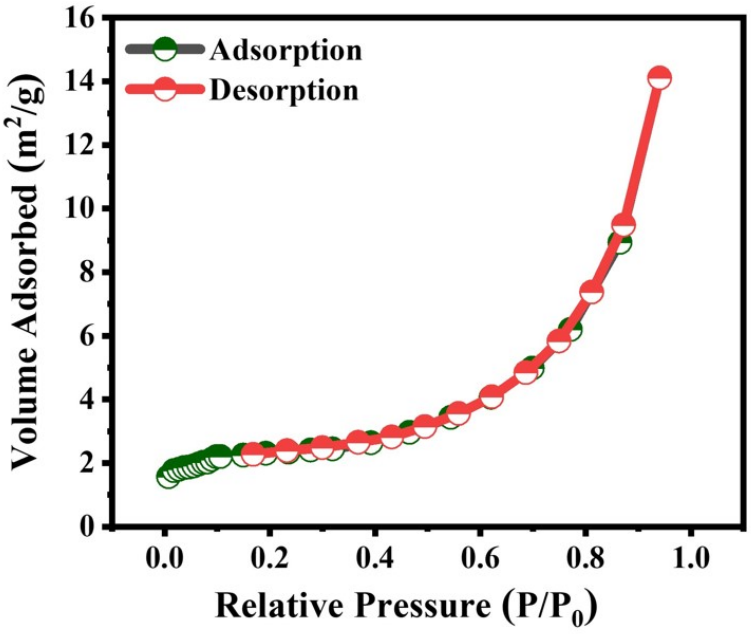


**Fig. S5.** Nitrogen adsorption-desorption isotherm curves of Cu NPs.

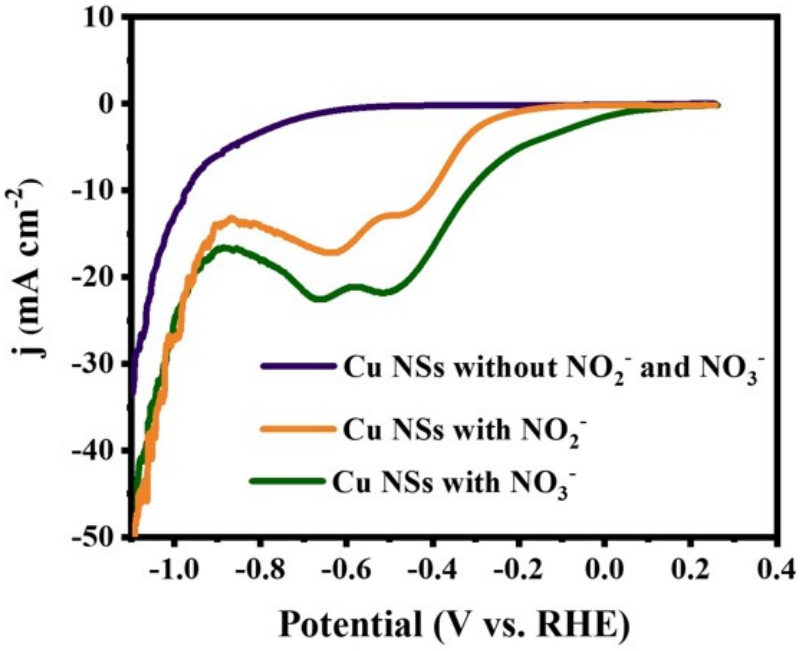


**Fig. S6.** LSV curves of Cu NSs in 0.5M $Na_2SO_4$ with $NO_2^-$ and $NO_3^-$.

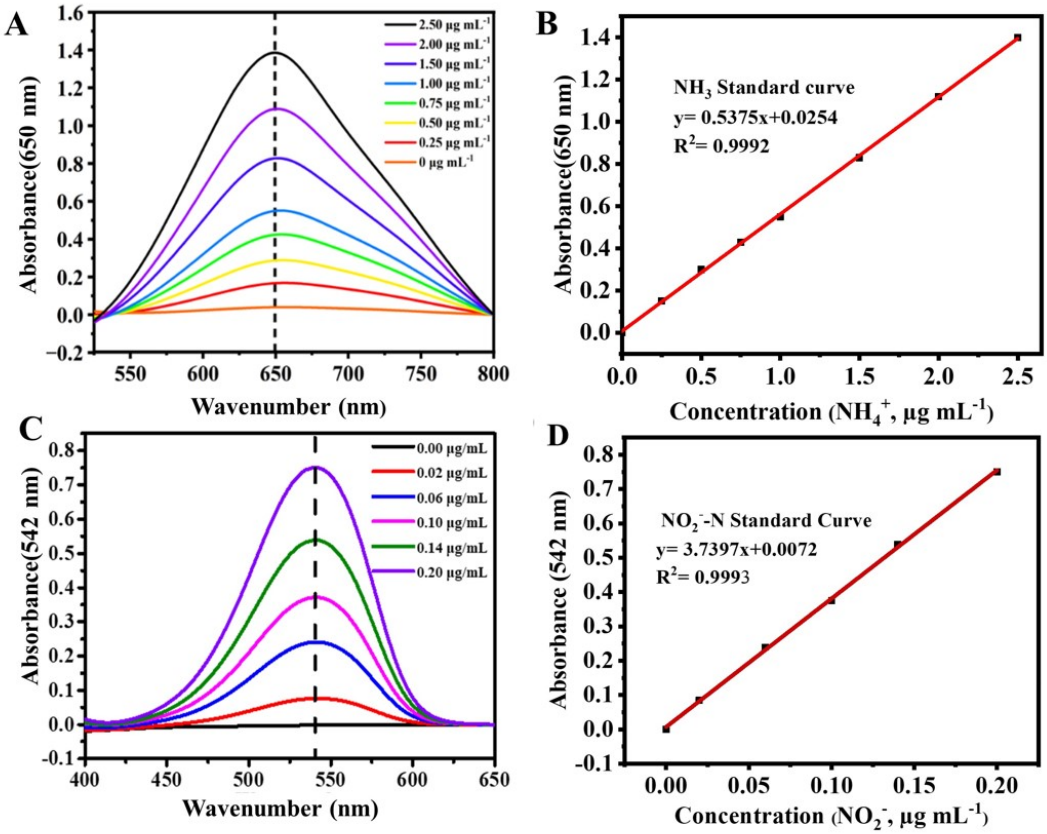


**Fig. S7.** (A) UV-vis curves of phenate assays after in darkness for 3 h at room temperature. (B) The calibration curve used for estimation of $NH_3$ by $NH_4^+$-N ion concentration. (C) UV-vis adsorption curves and (D) calibration curves of $NO_2^-$.

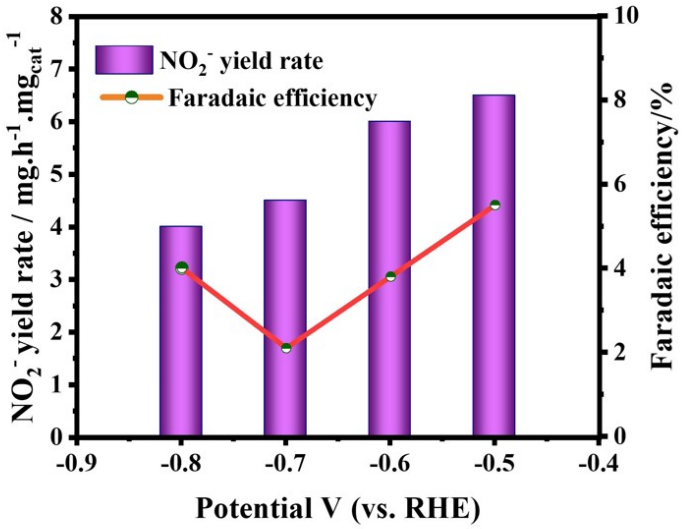


**Fig. S8.** The Faradaic efficiency and $NO_2^-$ yield on Cu NSs at different potential.

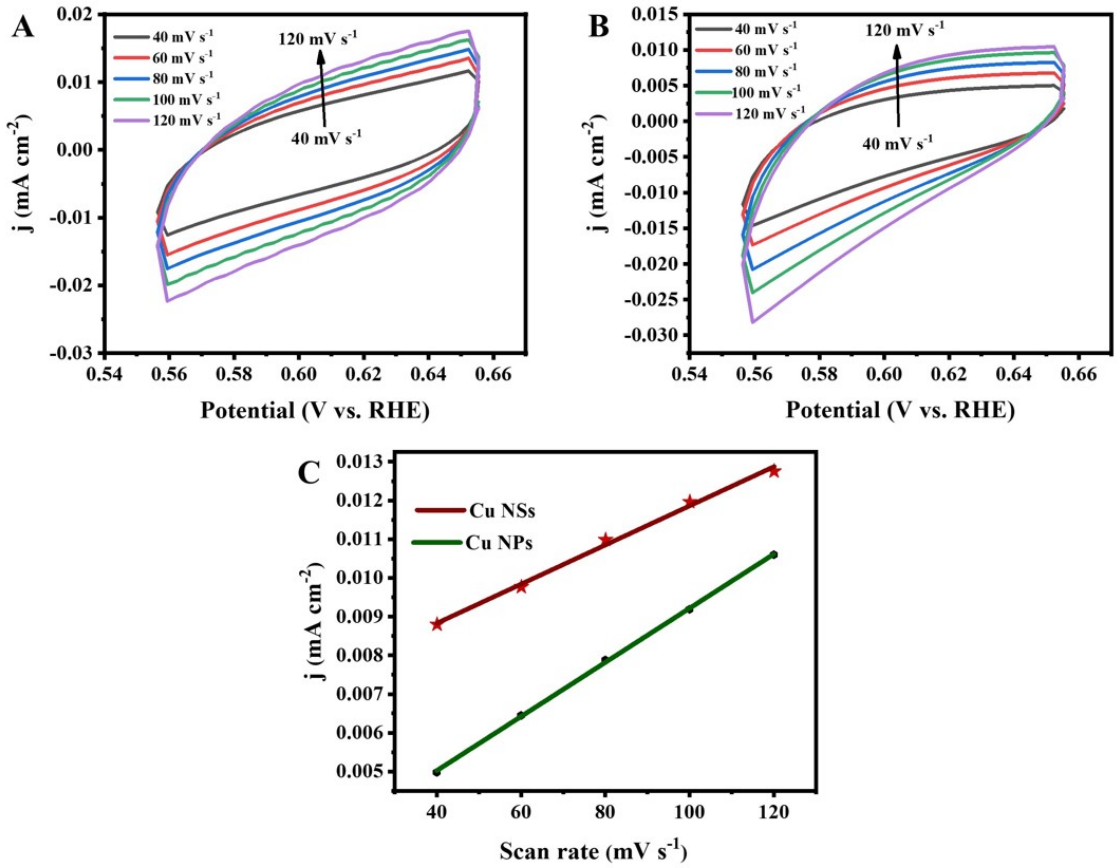


**Fig. S9.** CV curves of (A) Cu NSs (B) Cu NPs at different potential scanning rates in 0.5 M $Na_2SO_4$ solution. C) Linear fitting of $\Delta j$ of Cu NSs and Cu NPs ($\Delta j = j_a - j_c$) *vs.* scan rates at -0.7 V *vs.* RHE.

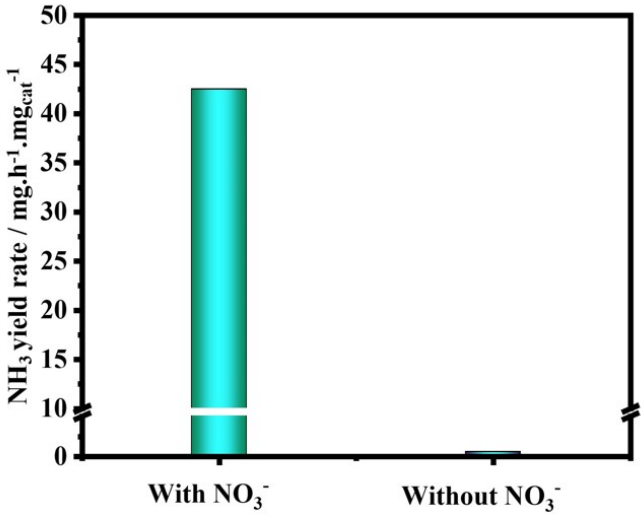


**Fig. S10.** The $NH_3$ yield on Cu NSs in 0.5 M $Na_2SO_4$ electrolyte with and without $NO_3^-$.

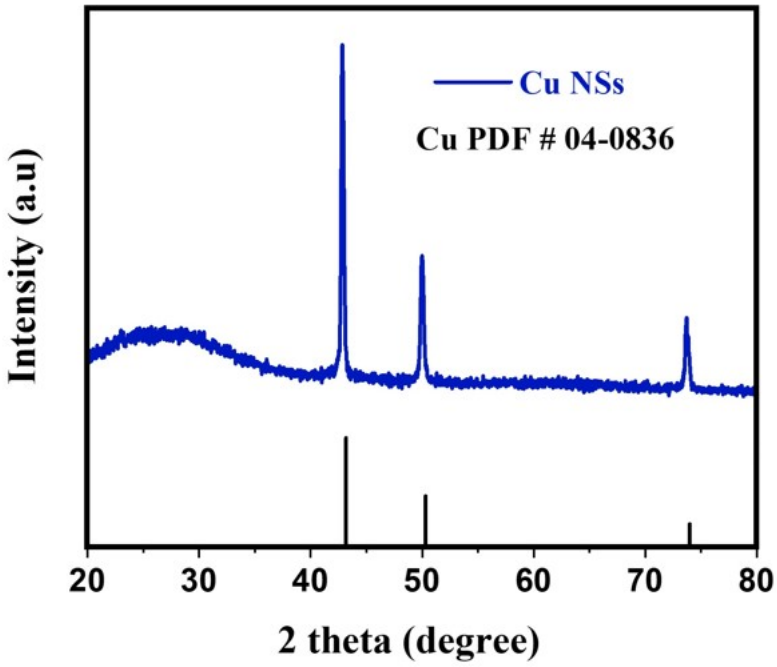


**Fig. S11.** XRD pattern of Cu NSs after chronoamperometry in 0.5 M $Na_2SO_4$ with 50 mM $NaNO_3$ at -0.7 V potential.

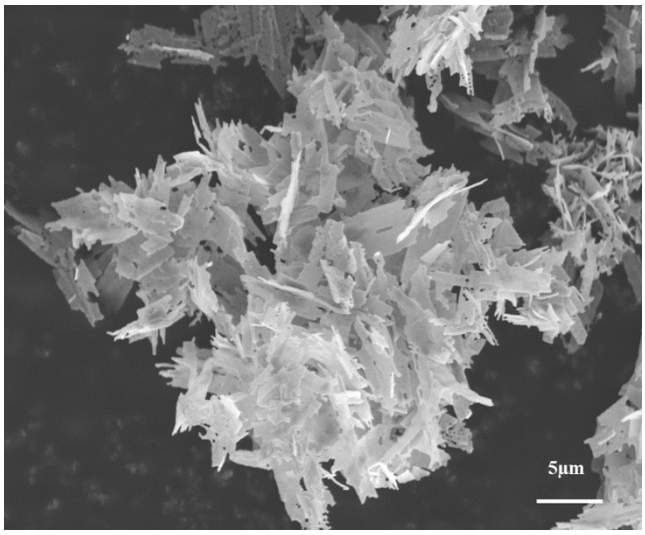


**Fig. S12.** SEM image of Cu NSs after chronoamperometry.

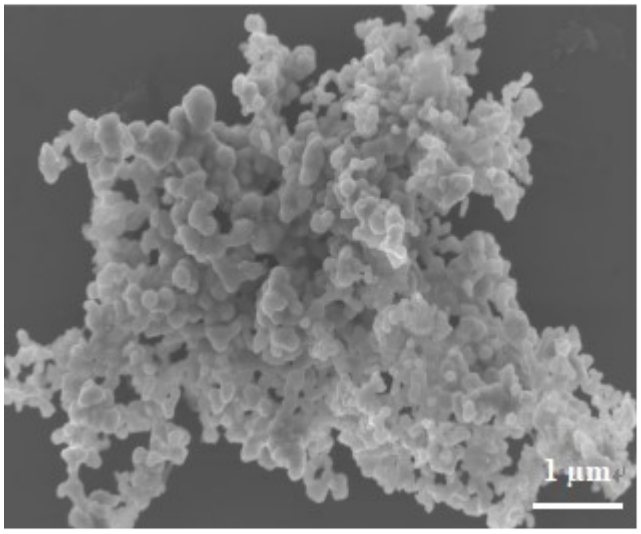


**Fig. S13.** SEM image of Cu NPs after chronoamperometry.

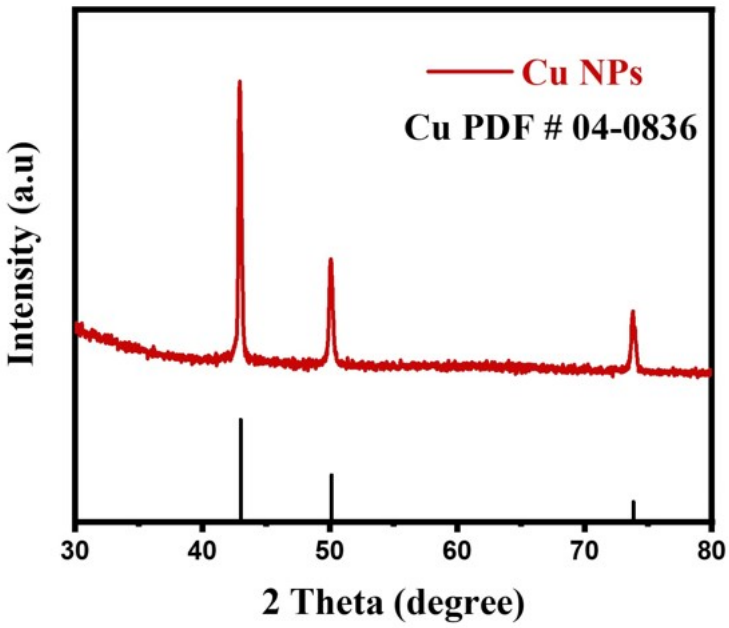


**Fig. S14.** XRD pattern of Cu NPs after chronoamperometry in 0.5 M $Na_2SO_4$ with 50 mM $NaNO_3$ at -0.7 V potential.

**Table S1** Comparisons of the $NO_3RR$ Activity of Electrocatalysts.

| Electrocatalysts | Electrolyte | Potential | $NH_3$ yield | FE (%) | Ref. (year) |
|---|---|---|---|---|---|
| Cu Nanosheet | 0.5 M $Na_2SO_4$ + 50 mM $NaNO_3$ | -0.70 V | 42.5 mg $h^{-1}$ $mg_{cat}^{-1}$ | 97.0 | This work |
| $Co_1$-P/NPG | 0.5 M $Na_2SO_4$ + 0.1 M $KNO_3$ | -0.7 V | 8.6 mg $h^{-1}$ $mg_{cat}^{-1}$ | 93.8 | 2024[3] |
| $Cu_xO$/N-GDY | 0.1 M KOH + 0.1 M $KNO_3$ | -0.5 V | 340 μmol $h^{-1}$ $mg_{cat}^{-1}$ | 85 | 2024[4] |
| Cu/$Cu_2O$/Pi | 1 M KOH +0.1 M $KNO_3$ | -0.5 V | 8.19 mg $h^{-1}$ $cm^{-1}$ | 96.6 | 2024[5] |
| Fe/Cu | 1 M KOH + 0.1 M $KNO_3$ | -0.5 V | 1.08 mmol $h^{-1}$ $mg^{-1}$ | 92.51 | 2023[6] |
| Cu-doped $Fe_3O_4$ flakes | 0.1 M KOH + 0.1 M $KNO_3$ | -0.6 V | 179.55 ± 16.37 mg $h^1$ $mg_{cat}^{-1}$ | ~100 | 2023[7] |
| CFP-$Cu_1Ni_1$ | 0.5 mol·$L^{-1}$ $Na_2SO_4$ + 0.1 mol·$L^{-1}$ $KNO_3$ | -0.22 V | 2550 μmol·$h^{-1}$·$mg_{cat}^{-1}$ | 95.7 | 2023[8] |
| Ru@$C_3N_4$/Cu NWs | 0.5 m $Na_2SO_4$ + 200 ppm $NO_3^-$ | -0.9 V | 0.249 mmol $h^{-1}$ $cm^{-1}$ | 91.3 | 2023[9] |
| $Cu_2O$/Cu $(OH)_2$ | 0.1 M KOH +500 ppm $NO_3^-$ | -0.6 V | 1.63 mg $h^{-1}$ $mg_{cat}^{-1}$ | 76.95 | 2024[10] |
| Cu/$Cu_{2+1}O$ NSA | 0.5 M $Na_2SO_4$ + 200 mg $L^{-1}$ $NO_3^-$ | -1.5 V | 0.2634 mmol $h^{-1}$ $cm^{-2}$ | 88.0 | 2024[11] |
| Cu MNC | 50 Mm $Na_2SO_4$ + 100 mg $L^{-1}$ $NaNO_3$ | -0.64 V | 5466 mmol $g_{Cu}^{-1}$ $h^{-1}$ | 65.3 | 2022[12] |
| $Cu_2O$ h-NCs | 0.5 M $Na_2SO_4$ + 0.05 M $NaNO_3$ | -0.85 V | 56.2 mg $h^{-1}$ $mg_{cat}^{-1}$ | 92.9 | 2022[13] |
| $Cu_2O$ | 0.5 M $Na_2SO_4$ + 5.0 mM $NaNO_3$ | -0.8 V | N/A | 92.28 | 2022[14] |
| Rh@Cu | 0.1 M $Na_2SO_4$ + 0.1 M $NaNO_3$ | -0.2 V | 21.59 mg $cm^{-2}$ $h^{-1}$ | 93 | 2022[15] |

## Reference:

(1) Y. Wang, W. Zhou, R. Jia, Y. Yu and B. Zhang, Unveiling the Activity Origin of a Copper-based Electrocatalyst for Selective Nitrate Reduction to Ammonia, *Angew. Chem. Int. Ed.,* 2020, **59**, 5350-5354.

(2) J. Zhu, Q. Xue, Y. Xue, Y. Ding, F. Li and P. Jin, Iridium Nanotubes as Bifunctional Electrocatalysts for Oxygen Evolution and Nitrate Reduction Reactions, *ACS. Appl. Mater. Interfaces.,* 2020, **12**, 14064-14070.

(3) J. Ni, J. Yan, F. Li, H. Qi, Q. Xu and C. Su, Atomic Co-P Catalytic Pair Drives Efficient Electrochemical Nitrate Reduction to Ammonia, *Adv. Energy Mater.,* 2024, **14**, 2400065.

(4) J. Li, R. Valenza and S. Haussener, In Situ Synthesis of $Cu_xO$/N Doped Graphdiyne with Pyridine N Configuration for Ammonia Production via Nitrate Reduction, *Small,* 2024, **20,** 2310467.

(5) W. Luo, Z. Guo, L. Ye, S. Wu, Y. Jiang and P. Xu, Electrical-Driven Directed-Evolution of Copper Nanowires Catalysts for Efficient Nitrate Reduction to Ammonia, *Small,* 2024, **20**, 2311336.

(6) S. Zhang, J. Wu, M. Zheng, X. Jin, Z. Shen and Z. Li, Fe/Cu Diatomic Catalysts for Electrochemical Nitrate Reduction to Ammonia, *Nat. Commun.,* 2023, **14**, 3634.

(7) J. Wang, Y. Wang, C. Cai, Y. Liu, D. Wu and M. Wang, Cu-Doped Iron Oxide for the Efficient Electrocatalytic Nitrate Reduction Reaction, *Nano Letters.,* 2023, **23,** 1897-1903.

(8) Z. Zhang, Y. Liu, X. Su, Z. Zhao, Z. Mo and C. Wang, Electro-Triggered Joule

Heating Method to Synthesize Single-Phase CuNi Nano-Alloy Catalyst for Efficient Electrocatalytic Nitrate Reduction Toward Ammonia, *Nano Res.,* 2023, **16**, 6632-6641.

(9) Y. Zheng, M. Qin, X. Yu, H. Yao, W. Zhang and G. Xie, Constructing Ru@$C_3N_4$/Cu Tandem Electrocatalyst with Dual-Active Sites for Enhanced Nitrate Electroreduction to Ammonia, *Small,* 2023, **19**, 2302266.

(10) N. Roy, P. C. Mandal, N. D. Sherpa, H. Barma and B. Adhikary, Electrochemical Nitrate Reduction to $NH_3$ by Faceted $Cu_2O$ Nanostructures in Acidic Medium, *New. J. Chem.,* 2024, **48**, 20384-20398

(11) C. Sun, Y. Xiao, X. Liu, J. Hu, Q. Zhao and Z. Yin, Three-Dimensional Porous Cu/$Cu_{2+1}O$ Nanosheet Arrays Promote Electrochemical Nitrate-to-Ammonia Conversion, *Inorg. Chem.,* 2024, **63**, 11852-11859.

(12) Y. Xue, Q. Yu, Q. Ma, Y. Chen, C. Zhang and W. Teng, Electrocatalytic Hydrogenation Boosts Reduction of Nitrate to Ammonia Over Single-Atom Cu with Cu(I)-$N_3C_1$ Sites, *Environ. Sci. Technol.,* 2022, **56,** 14797-14807.

(13) X. Wang, Z. Wang, Q. Hong, Z. Zhang, F. Shi and D. Li, Oxygen-Vacancy-Rich $Cu_2O$ Hollow Nanocubes for Nitrate Electroreduction Reaction to Ammonia in a Neutral Electrolyte, *Inorg Chem.,* 2022, **61,** 15678-15685.

(14) C. Wang, F. Ye, J. Shen, K. Xue, Y. Zhu and C. Li, In Situ Loading of $Cu_2O$ Active Sites on Island-Like Copper for Efficient Electrochemical Reduction of Nitrate to Ammonia, *ACS Appl. Mater. Interfaces.,* 2022, **14,** 6680-6688.

(15) H. Liu, X. Lang, C. Zhu, J. Timoshenko, M. Ruscher and L. Bai, Efficient Electrochemical Nitrate Reduction to Ammonia with Copper-Supported Rhodium

Cluster and S-Atom Catalysts, *Angew. Chem. Int. Ed.,* 2022, **61**, e202202556.